Title: Aerosol scattering and absorption Angström exponents as indicators of dust and dust-free days over Granada (Spain)
Author(s): Valenzuela, A.; Olmo, F.J.; Lyamani, H.; M. Antón, G.Titos, A. Cazorla and L. Alados-Arboledas
Source: Atmospheric Research Volume: 154 Pages: 1-13 Published: 2015
Times Cited: 33
DOI: 10.1016/j.atmosres.2014.10.015

AEROSOL SCATTERING AND ABSORPTION ANGSTRÖM EXPONENTS AS INDICATORS OF DUST AND DUST-FREE DAYS OVER GRANADA (SPAIN)

A.Valenzuela[1,2], F.J. Olmo[1,2], H. Lyamani[1,2], M. Antón[3], G.Titos[1, 2] A. Cazorla[1, 2] and L. Alados-Arboledas[1,2]

[1] Departamento de Física Aplicada, Universidad de Granada, Fuentenueva s/n, 18071-Granada, Spain

[2] Grupo de Física de la Atmósfera. IISTA. Universidad de Granada, Granada, Spain

[3] Departamento de Física, Universidad de Extremadura, Av. Elvas s/n, 06071-Badajoz, Spain

Corresponding author: Antonio Valenzuela, Departamento de Física Aplicada, Universidad de Granada, 18006 Granada Spain.

e-mail: avalenzuela@ugr.es

Keywords: desert dust events, anthropogenic aerosol, passive remote sensing, in situ instruments, aerosol scattering and absorption Angström exponents.

ABSTRACT

This paper focuses on the assessment of atmospheric aerosol optical properties at the surface and in atmospheric column during both desert dust and dust-free conditions over Granada, South-eastern Iberian Peninsula. Indeed, the spectral dependence of aerosol absorption and scattering properties are analyzed in detail. The analyzed period ranges from June 2008 to December 2010. On dusty days, the mean scattering Angström exponent value obtained in the atmospheric column (SAE^{col}) (0.5±0.3) was lower than the observed at the surface level (SAE^{is}) (1.3±0.6), indicating higher contribution of coarse particles at high atmospheric level than at ground level during the analyzed dust events. In addition, it is noticed that the absorption Angström exponent in the atmospheric column (AAE^{col}) with mean value of 1.5±0.2 and at the surface (AAE^{is}) with mean value of 1.3±0.2 obtained during dusty situations are indicative of mixture of desert dust and black carbon particles as dominant absorbers both in the atmospheric column and at the surface during dust intrusions over Granada. On the other hand, a non-parametric test (Kolmogorov-Smirnov) revealed that no significant statistical difference was found for AAE^{is} between desert dust and free-dust conditions. This result may be due to the important contribution of urban absorbing

aerosol (e.g. Black carbon) at ground level in the study location. Therefore, these parameters (AAE^{col} and AAE^{is}) are not very useful to detect desert dust events without the use of other information (e.g., aerosol size) over urban area like Granada.A dust extreme event was analyzed in order to retrieve optical parameters during situation dominated by desert dust. The values of SAE^{col} and SAE^{is} obtained during this extreme event were in agreement with the values showed above for the period 2008-2010, although the differences between dust-free and dust conditions are more noticeable in this special event.

1. INTRODUCTION

There is great difficulty in characterizing the aerosol optical and microphysical properties resulting in a large uncertainty in the radiative forcing of climate. The impact of atmospheric aerosols on radiative forcing is still remaining highly uncertain due to their great spatial and temporal variability and the large variability in composition, size distribution, particle shape and vertical distribution (IPCC, 2013). Part of this uncertainty is associated with the large uncertainty in individual radiative forcing for several aerosol components, such as black carbon and desert dust (IPCC, 2013). The Aerosol Optical Depth (AOD) and the Extinction Angström Exponent (EAE) (Angström, 1929) are two important properties of atmospheric aerosols. AOD gives information about the aerosol load while EAE is related with the particle size (Costabile et al., 2013). Values of EAE higher than 1 indicate fine particle predominance and values lower than 1 indicate that coarse particles are predominant. However, EAE is not an ideal indicator of the exact average size of particles as it also dependents on aerosol absorption (Kaskaoutis and Kambezidis, 2008). In this sense, another relevant aerosol property is the Absorption Angström Exponent (AAE) which gives information about absorbing particle types (e.g. Russell et al., 2010). This parameter is defined as the slope of a log-log plot of the Aerosol

96 Absorption Optical Depth (AAOD) versus wavelength (Russell et al., 2010; Eck et al.,
97 2010). Values of the AAE close to 1 are referred to pure black carbon while dust particles
98 present, generally, AAE values larger than 2 (e.g, Bergstrom et al., 2004; Bergstrom et al.,
99 2007; Bergstrom et al., 2010). However, AAE values depend on the wavelength range
100 considered for its determination (e.g. Russell et al., 2010). These last authors found that
101 AAE is 1.45 over the range 325-1000 nm, but 1.11 over the range 325-1685 nm for
102 biomass burning in southern Africa. They reported AAE values above 2 in the wavelength
103 range 440-670 nm and values around 1.6 on the range 440-1020 nm at Solar Village (a
104 desert location in Saudi Arabia). Lack and Cappa (2010) showed that the coating on the
105 BC particles leads to AAE as high as 1.6 due to non-absorbing coating. Therefore, these
106 literature results make difficult the attribution of observed light absorption to a specific
107 aerosol absorbing type. Thus, it is necessary to define other variables to use them
108 together with the AAE in order to obtain more information about the aerosol type. In this
109 sense, the Scattering Angström Exponent (SAE) is used to evaluate the scattering of solar
110 radiation due to atmospheric aerosols. This parameter depends primarily on the particles
111 size and ranges from 4 (Rayleigh atmosphere) to 0 (large particles).
112 Several studies have focused on the determination of AAE values by means of

columnar optical properties: sun/sky radiance data (e.g., Eck et al., 2010; Russell et al., 2010), combined measurements of the spectral solar radiation and the spectral aerosol optical depth (e.g, Bergstrom et al., 2007; Bergstrom et al., 2010). Other studies focused on AAE values obtained using in situ measurements (e.g., Yang et al., 2009; Soni et al., 2010; Lee et al., 2012). Generally, the AAE and SAE values (columnar/in situ) are different; however, it is interesting to investigate the simultaneous columnar and in situ measurements of these parameters in order to check the aerosol properties reproducibility in both levels. However, very sparse studies focused on AAE and SAE obtained simultaneously both on the ground level and in the atmospheric column. In order to establish the connection between the AAE, SAE and the aerosol source, Cazorla et al. (2013) combined columnar sun/sky radiance data with optical and chemical properties retrieved in situ from aircraft campaigns. On the other hand, Kim et al. (2005) employed simultaneous sun-photometer and in-situ measurements to obtain aerosol optical, chemical and physical properties during dust and pollution episodes at Gosan (Korea). Continuous measurements recorded during the SAMUM campaign (May/June 2006, Morocco) provided an excellent opportunity to analyze the aerosol properties retrieved both at surface and in the atmospheric column close to desert dust sources (Schladitz et al.,

130 2009; Knippertz et al., 2009; Tesche et al., 2009).

131 Another relevant parameter to quantify the absorption properties of the atmospheric
132 aerosol is the single scattering albedo ($\omega(\lambda)$), which is the ratio of scattering to extinction.
133 The spectral dependence of $\omega(\lambda)$ is driven by the spectral dependence of both absorption
134 and scattering (e.g. Dubovik et al. 1998). Valenzuela et al. (2012a; 2012b) have evaluated
135 the atmospheric columnar aerosol optical and radiative properties during desert dust
136 intrusions at Granada (Spain). These authors found that columnar aerosol single
137 scattering albedo was lower than in others worldwide locations which they attributed:
138 firstly, to the mixing of desert dust with particles anthropogenic particles during their
139 transport over Mediterranean polluted areas as well as urban-industrialized North African
140 areas, and secondly, to the influence of pollutants emitted locally or regionally.
141 Furthermore, these authors showed that the mixtures of desert dust aerosol and
142 anthropogenic particles lead to a large variability in the spectral dependence of $\omega(\lambda)$.

143 Due to its geographical situation, Granada city is an interesting place to analyze the
144 atmospheric aerosol optical properties using different methodologies: in-situ and remote
145 sensing instrumentation. The main aim of this work is the assessment of aerosol optical
146 properties during desert dust events and dust-free conditions in atmospheric column and

147 at the surface over Granada from 2008 to 2010. For this purpose, measurements obtained
148 by passive remote sensing (sunphotometer CIMEL) and ground-based “in situ”
149 instruments (integrating nephelometer and Particle Soot Absorption Photometer, PSAP)
150 are used.

151 ## 2. EXPERIMENTAL SITE

152 Measurements performed in Granada (37.18ºN, 3.58ºW and 680 m a.s.l) from June
153 2008 to December 2010, when both in-situ and column measurement were available, are
154 used in this study. Granada is located in South-eastern Spain, and it is a non-industrialized
155 medium-sized city with a population of about 250,000 inhabitants that increases up to 300,000
156 when the metropolitan area is included. The city is situated in a natural basin surrounded by
157 mountains with altitudes over 1000 m. The near-continental conditions prevailing at this site
158 are responsible for large seasonal temperature differences, providing cool winters and hot
159 summers. The study area is also about 200 km away from the African continent, and
160 approximately 50 km away from the western Mediterranean basin. Due to its location in
161 the Mediterranean basin, Granada is influenced by two major aerosol source regions:
162 Europe as a major source of anthropogenic pollutants and North Africa as principal source
163 of natural dust (Lyamani et al, 2005, 2006; Valenzuela et al., 2012a). In addition, the
164 station is located in the southern part of the city and is about 500m away from the highway

165 that surrounds the city and about a similar distance from one of the principal traffic roads
166 of the city. The local aerosol sources are mainly the heavy traffic together with the re-
167 suspension of material available on the ground (Lyamani et al., 2008; 2010).
168
169 ## 3. INSTRUMENTATION AND METHODS
170 ### 3.1 Surface in situ instruments
171 Air sampling for all the in situ instruments was obtained from the top of a stainless
172 steel tube, 20-cm diameter and 5-m length (Lyamani et al., 2008). The inlet is fitted with a
173 funnel and covered by an insect screen to prevent rain drops and insects from getting into
174 the sample line. The inlet was located about 15 m above the ground. Measurements were
175 performed with no aerosol cut-off and no heating was applied to the sampled air. There is
176 no bend in the tube that passes through the rooftop. Several stainless-steel pipes located
177 inside the stainless steel tube provided sample air to the different instruments.
178 The aerosol scattering coefficients (σ_{sp}) were measured at three wavelengths (450,
179 550 and 700 nm) with an integrating nephelometer (TSI model 3563). Calibration of the
180 nephelometer was carried out every three months using CO_2 as a high span gas and
181 filtered air as a low span gas. The averaging time was set to 5 min. The zero signals were

182 measured hourly. The raw σ_{sp} data were corrected for truncation and non-Lambertian
183 illumination errors were corrected using the method described by Anderson and Ogren
184 (1998). The uncertainty in σ_{sp} is of 7% (Heintzenberg et al., 2006).

185 The aerosol absorption coefficients (σ_{ap}) were measured with a Particle Soot
186 Absorption Photometer (PSAP). The PSAP instrument provides measurement of the light
187 absorption by aerosol particles that are collected on a filter (Bond et al. 1999). Here, a 3-
188 wavelength version of the PSAP has been used, with measurements at 467 nm, 531nm,
189 and 650 nm. The PSAP data require the corrections of the aerosol light scattering and the
190 filter loading effects on the measurement of the aerosol absorption coefficient. In this
191 study, the correction proposed by Bond et al. (1999) and further adapted by Ogren et al.
192 (2010) to 3-λ PSAP was used to correct the PSAP data. The PSAP was operated at a flow
193 rate of 1.5 l min^{-1}. The averaging time was set to 1 min. The uncertainty of the PSAP
194 absorption measurement, after application of the transmission and scattering correction, is
195 20–30% (Bond et al. 1999). The detection limit of this instrument is 1.8 Mm^{-1} with an
196 averaging time of 1 min. PSAP data were averaged over the same time period as the
197 nephelometer.

198 Absorption coefficients (σ_{ap}) obtained at three wavelengths (467, 531 and 650 nm) were

used to derive the absorption Angstrom exponent (AAE^{is}) employing the Angström relationship (Angström, 1929):

$$AAE^{is}(\lambda)=-(\ln(\sigma_{ap}(\lambda_1)/\sigma_{ap}(\lambda_2))/\ln(\lambda_1/\lambda_2)) \quad (1)$$

where $\sigma_{ap}(\lambda)$ is the absorption coefficient at a specific wavelength, λ , and AAE^{is} is the absorption Angstrom exponent. The superscript "is" means that this parameter has been retrieved from surface in situ measurements.

The AAE^{is} was calculated using σ_{ap} measured at 467 and 650 nm wavelengths. Values of AAE^{is} close to the unity are related to the BC particles dominance. Whereas values of $AAE^{is} \geq 1.5$ are indicative of the presence of dust or brown carbon particles.

The scattering Angström exponent (SAE^{is}) is derived from equation 1 but using scattering coefficients instead of absorption coefficients. SAE^{is} larger than 1.5 indicates an aerosol size distribution with scattering dominated by submicron particles, while a distribution dominated by coarse particles has typically SAE^{is} smaller than 1. The SAE^{is} was calculated using σ_{sp} measured at 450 and 700 nm wavelengths. Using the Angström relationship, the σ_{ap} values at 467, 531, and 650 nm were interpolated using the AAE^{is} derived from the PSAP data to the nephelometer wavelengths 450, 550, and 700 nm.

The uncertainty associated to the AAE^{is} and SAE^{is} has been calculated following the

procedure described in Rizzo et al. (2011) and it is estimated to be 20% for AAE^{is} and from 14% for SAE^{is}.

The scattering and absorption coefficients at 467, 531 and 650 nm were used to estimate the single scattering albedo at surface (ω^{is}) at the same wavelengths. The ω^{is} was estimated using the following equation:

$$\omega^{is}(\lambda)=(\sigma_{sp}(\lambda)/(\sigma_{sp}(\lambda)+\sigma_{ap}(\lambda))) \quad (2)$$

3.2 Passive remote sensing instrument

Measurements of total columnar aerosol properties were obtained using CIMEL CE-318 sun photometer included in the AERONET network (Holben et al., 1998). This sun-photometer makes direct sun measurements with a 1.2º full field of view at 340, 380, 440, 500, 670, 870 and 1020 nm. The full-width at half-maximum of the interference filters are 2 nm at 340 nm, 4 nm at 380 nm and 10 nm at all other wavelengths. The sky radiance measurements (almucantar configuration) are carried out at 440, 670, 870 and 1020 nm. This instrument is fully described by Holben et al. (1998). The direct sun measurements are used to compute the aerosol optical depth (AOD) at 340, 380, 440, 670, 870 and 1020 nm (Holben et al., 1998). In this work, the AERONET AOD data of level 2 (cloud screened and quality assured) are used. The uncertainty in the retrieval of AOD under cloud free conditions is ±0.01 for wavelengths larger than 440 nm and ±0.02 for shorter wavelengths (Eck et al., 1999). The sky

radiance measurements in conjunction with solar direct irradiance measurements are used to retrieve aerosol microphysical properties like single scattering albedo, ω^{col}, using the AERONET inversion algorithm developed by Dubovik and King (2000) with improvements by Dubovik et al. (2006). The uncertainty in the retrieval of ω^{col} is ±0.03 for high aerosol load (AOD (440 nm) > 0.4) and solar zenith angle > 50°. For measurements with low aerosol load (AOD(440 nm) < 0.2), the retrieval accuracy of ω^{col} drops down to 0.02-0.07 (Dubovik et al., 2000). Due to the strong limitations imposed by the AERONET inversion algorithm (AOD (440 nm) > 0.4 and solar zenith angle > 50º) and the reduced sampling of almucantar sky radiance measurements as well as the presence of clouds during measurements, there were very few ω^{col} level 2 retrievals at Granada. Thus, the AERONET ω^{col} level 1.5 data (cloud screened data with pre and post calibrations applied) for AOD >0.2 and solar zenith angle > 50º are used here.

The Fine Mode Fraction (FMF) of AOD was computed based on the retrieved size distributions and spectral refractive indices from the Dubovik and King (2000) algorithm applied to AERONET almucantar scans, assuming bimodal size distributions. In this case we have computed FMF (670) as the ratio of AOD_{fine} (fine aerosol optical depth) to AOD (total aerosol optical depth) where AOD is the sum of fine aerosol optical depth and coarse aerosol optical depth.

The aerosol optical depths AOD and the single scattering albedos ω^{col} were used to

calculate the absorption optical depth AAOD (Rusell et al., 2010):

$$AAOD=(1-\omega^{col})\cdot AOD \quad (3)$$

The scattering aerosol optical depth (AOD_{scat}) was obtained by subtracting the absorption optical depth to the extinction optical depth.

The scattering Angström exponent (SAE^{col}) and the absorption Angström exponent (AAE^{col}) were computed using the Angström relationship and AOD_{scat} and AAOD in wavelength range 440-1020 nm. The superscript "col" means that these parameters have been retrieved for the atmospheric column.

3.3 Criteria for selection of desert dust and dust-free days

We have considered African dust events that affected the study site and were present at ground level as confirmed by CALIMA network (www.calima.ws). Thus, dust particles were present in the all atmospheric column in these dust event cases. For detecting the African desert dust intrusions over Iberian Peninsula, CALIMA network uses models as SKIRON, BSC-DREAM and NAAPs as well as back-trajectories analysis by HYSPLIT4 model (Draxler et al., 2009), synoptic meteorological charts, satellite images, and surface data (PM10 levels recorded at regional background stations from air quality

monitoring). On the other hand, sun-photometer measurements have also been analyzed to confirm the desert dust intrusions over Granada. An abrupt increase in the AOD associated with a sharp decrease in the SAE^{col} is indicative of the presence of desert dust over the study area (Lyamani et al., 2005, Valenzuela et al., 2012). Also, we have performed a back trajectories analysis of air masses arriving to Granada at three different levels, 500, 1500 and 3000 m a.g.l to identify their origins and pathways.

Regarding dust-free days, we have considered those days not included by CALIMA network as dusty. In addition, we have established the criterion of $SAE^{col}>1.0$ for dust-free conditions. Furthermore, we have checked the air masses back trajectories to confirm that the air masses on these days did not arrive from North Africa.

4. RESULTS AND DISCUSSION

4.1. Spectral single scattering albedo, scattering and absorption Angström exponents.

The ratio of scattering to extinction (sum of scattering and absorption) is defined as the single scattering albedo. This parameter is an intensive property determined by the particle composition and size and represents a relevant variable in climate modeling (e.g. Bodhaine, 1995). Figure 1 shows the mean values of single scattering albedo and their standard deviations retrieved from columnar measurements (computed in the spectral

289 range 440-1020 nm) and computed from surface in situ measurements (computed in the
290 spectral range 467-650 nm) during desert dust and dust-free conditions. Only coincident
291 instantaneous values of single scattering albedo at surface and in the atmospheric column
292 are used in the calculation of the mean values. These mean values of single scattering
293 albedo were calculated from 280 and 2422 simultaneous measurements during dusty and
294 free conditions, respectively. During desert dust events, mean ω^{col} values exhibited a weak
295 increase with wavelength. The mean ω^{col} values and the corresponding standard
296 deviations of this parameter were 0.89 ± 0.03 at 440 nm and 0.96 ± 0.03 at 1020 nm. This ω^{col}
297 spectral dependence behavior was reported in other studies for desert dust events (e.g.,
298 Collaud Coen et al., 2004; Lyamani et al., 2006; Alados-Arboledas et al., 2008; Cachorro
299 et al., 2008; Su and Toon, 2011; Toledano et al., 2011). The increase of ω^{col} with
300 wavelength is a typical pattern for dust particles (e.g. Lyamani et al., 2006; Valenzuela et
301 al., 2012) due to the spectral absorption properties of iron oxides in ultraviolet-visible
302 spectral region (Sokolik and Toon, 1999). However, in our study, ω^{col} values in 440-1020
303 nm spectral range were lower than those obtained in other studies during desert dust
304 intrusions over or near desert dust sources (e.g. Tamanrasset and Solar Village) (Table 1).
305 However, the columnar single scattering albedo values recorded in our study during dust

306 intrusions were comparable to those obtained over Lecce (40.33ºN, 18.10º E), in the Central
307 Mediterranean, during desert dust events associated with significant contribution of
308 anthropogenic absorbing particles (Table 1). Thus, the results obtained in our study
309 suggest a significant contribution of anthropogenic absorbing particles from local or
310 regional origin during the analyzed desert dust intrusions over Granada.

311 The spectral behavior of ω^{col} obtained under dust-free conditions showed opposite
312 trend to the observed in desert dust cases. Indeed, the mean ω^{col} values decreased as the
313 wavelength increases, ranging from 0.90±0.03 at 440 nm to 0.86±0.03 at 1020 nm. This is
314 a typical ω^{col} spectral characteristic of an urban-industrial aerosol (e.g. Dubovik et al.,
315 2002b; Eck et al., 2001a; 2001b). The ω^{col} values obtained here under dust-free conditions
316 were similar to those observed by Lyamani et al. (2006) during anthropogenic events over
317 Granada (Table 1).

318 The mean ω^{is} values calculated from surface in situ measurements of absorption
319 and scattering coefficients showed almost neutral variation with wavelength during desert
320 dust events (Figure 1). The mean ω^{is} values and the corresponding standard deviations of
321 this parameter were 0.74±0.09 at 467 nm and 0.76±0.09 at 650 nm. This neutral spectral
322 dependency can be related to the increased contribution of absorbing particles from local

anthropogenic activities (domestic heating based on fuel oil combustion and vehicular emission) near surface. These values were lower than those obtained in Gosan, Korea and in Beijing, China during desert dust episodes observed at ground level (Table 1).

Under dust-free conditions the mean ω^{is} showed almost neutral dependence with wavelength at the surface because the difference of mean ω^{is} values at 467 and at 650 nm with 0.62±0.13 and 0.61±0.13, respectively, was within standard deviation. In general, the mean ω^{is} values obtained in our study site were smaller than those obtained in Delhi, Toulon, and Guangzhou (Table 1). The significantly low values of ω^{is} recorded at Granada under dusty and dusty free conditions indicate a large absorbing aerosol fraction in the aerosol population near surface over this region, which consequently will have implications on the regional radiative forcing.

The mean $AOD_{scat}(\lambda)$ values obtained by sun-photometer and the mean σ_{sp} values measured by the nephelometer during dust and dust-free conditions and their corresponding standard deviations are shown in Figure 2(a,b). Only coincident instantaneous values obtained at surface and in the atmospheric column are used in the calculation of the mean values. The mean SAE^{col} value (computed in 440-1020 nm spectral range) obtained during desert dust events was of 0.5±0.2, indicating atmospheric

column dominated by coarse particles. However, the mean SAE^{is} value (computed in 450-700 nm spectral range) obtained at surface during dust events was of 1.3±0.6, indicating higher contribution of coarse particles at high atmospheric level than at ground level during the analyzed dust events. This result is in agreement with previous studies performed at Granada, showing that usually desert dust is transported at high altitude over Granada (Granados et al, 2014; Cordona-Jabonero et al., 2011; Guerrero-Rascado et al., 2009). The mean SAE^{is} value (1.3±0.6) obtained during desert dust events over Granada was larger than those obtained in Beijing (China) and Gosan (Korea) during desert dust intrusions (Table 1). Also, the mean SAE^{col} value obtained under dusty conditions is slightly higher than that obtained during dust events at Gosan, Korea (Table 1). This difference can be related to the major contribution of the fine particles during desert dust events over Granada as compared to Gosan or differences in dust intensity. On the other hand, the mean SAE^{is} value was of 1.6±0.4 under dust-free conditions, indicating aerosol size distributions with scattering dominated by submicron particles. In the atmospheric column, the mean SAE^{col} value was of 1.2±0.4 during dust-free conditions. The significant contribution during dust-free conditions of fine anthropogenic particles was more evident at surface according to the mean SAE^{is} value. These values of SAE^{col} and SAE^{is} obtained

357 under urban pollution influence were almost similar to those obtained in Gosan, Korea
358 (Table 1).

359 In the absence of information on the aerosol chemical composition, the values of
360 AAE^{col} and AAE^{is} have been used as an indicator of the dominant absorbing particles type
361 in the aerosol population (e.g. Rusell et al., 2010; Cazorla et al., 2013). For pure black
362 carbon particles AAE^{col} (AAE^{is}) are typically close to the unity (e.g. Bergstrom et al., 2007).
363 Lack and Cappa (2010) established that Absorption Angström Exponent values ranging
364 between 1 and 1.6 can be attributed to black carbon particles coated by non-absorbing
365 particles and Absorption Angström Exponent higher than 1.6 can be associated with dust
366 or brown carbon. Giles et al. (2011) established that SAE^{col} ~0.5 with AAE^{col} ~1.5,
367 represents an optical mixture of fine mode black carbon and coarse mode dust as the
368 dominant absorbers. The mean AAOD values obtained by sun-photometer and the mean
369 σ_{ap} values measured by PSAP during dust and dust-free conditions and their
370 corresponding standard deviations are shown in Figure 3(a,b). The mean AAE^{col} value was
371 of 0.9±0.6 during dust-free conditions over Granada, suggesting that black carbon was the
372 principal absorber in the entire atmospheric column. This mean value was slightly lower
373 than the mean AAE^{col} values obtained by Giles et al. (2012) for urban-industrial aerosol in

374 Shirahama (1.1±0.5), Moldova (1.2±0.3) and Mexico City (1.3±0.3). The mean AAE^{is} value
375 obtained during dust-free conditions was of 1.4±0.3 which can be attributed to the black
376 carbon particles coated by non-absorbing particles (Lack and Cappa, 2010).
377 The mean AAE^{col} value obtained during dusty days was 1.5±0.2, which is higher
378 than the obtained during dust-free days. This result indicates a mixture of desert dust and
379 black carbon particles as the dominant absorbers in the atmospheric column during dust
380 intrusion over Granada (Giles et al., 2011). Similar mean AAE^{col} value was reported in
381 Solar Village (~1.6 on wavelength range 440-1020 nm) by Rusell et al. (2010). On the
382 other hand, the mean AAE^{is} value obtained during dusty days was of 1.3±0.2 which is
383 lower than the retrieved in the atmospheric column. The mean AAE^{is} value obtained
384 during dusty conditions was almost similar to that obtained in dust-free conditions
385 (1.4±0.3), probably due to the small dust (iron oxides) contribution at the surface during
386 the majority of analyzed dust events. As we mentioned before, Saharan dust is usually
387 transported at high altitude over Granada with less impact at ground level (Granados et al.,
388 2014; Cordoba-Jabonero et al., 2011; Guerrero et al., 2009). It is worth to note, however,
389 that during some occasional intense desert dust events at ground level AAE^{is} (SAE^{is}) can
390 reach values up to 2.5 (0.08) (see section 4.3). Therefore, in view of the results, AAE^{is} and

391 SAE^{is} parameters seem to be not useful for identifying dust particles during low-moderate
392 intense dust intrusions at ground level in urban locations as Granada with significant
393 anthropogenic aerosol presence.

394 The large range of SAE^{col} (SAE^{is}) and AAE^{col} (AAE^{is}) values obtained at Granada
395 is indicative of a wide range of particle size over this location in addition to various
396 absorbent components during desert dust events and dust-free influence. Thus, frequency
397 distributions of these two parameters in both column and surface during dusty and free
398 dust conditions are shown in Figure 4. During dusty situations, the SAE^{col} values were
399 below 1 in 90% of cases with a maximum around 0.5 (Figure 4a) indicating that coarse
400 particles were predominant. Up to 80% of observations showed values of AAE^{col} higher
401 than 1.4 (Figure 4b) during dusty days. These results were not reproduced at surface with
402 ground-based in situ instrumentation as we can see (Figures 4e and 4f) probably due to
403 the small impact of desert dust at surface in the majority of the analyzed dust events. The
404 SAE^{is} values ranged from 0 to about 2 with a maximum around 1.4 during desert dust
405 events indicating that for a significant number of observations Fine Mode Fraction (FMF)
406 dominate at surface (Figures 4e and 4f). Dust particles were predominant at ground level
407 (SAE^{is} <1) in only 44% of the observations (Figure 4e). On the other hand, the AAE^{is}

values obtained under dusty conditions ranged between 1 and 1.6 with an absolute maximum centered on 1.1 and a second maximum centered on 1.5. AAE^{is} values larger than 1.5 indicating the presence of dust at the surface were observed in only 15% of the observations. According to our previous comments, AAE^{col} values obtained in the atmospheric column under dusty conditions cannot be only attributed to dust, and therefore, other light absorbing materials also were responsible of absorption as black carbon (Giles et al., 2011). This fact could be due to two factors, the higher concentrations of fine absorbing particles near the surface and another one to the low iron oxide amounts during desert dust events. The concentration of fine absorbing particles probably increases during dust events which usually coincide with a stable meteorological situation that favor the air masses stagnation and the pollutants accumulation.

During dust-free conditions we found a maximum for SAE^{col} centered around 1.3 while AAE^{col} showed a maximum value centered on 1.0 (Figures 4c and 4d). At surface, AAE^{is} under dust free conditions showed a maximum value centered on 1.7 and a second maximum around 1.5, suggesting the important contribution of fine particles while AAE^{is} histogram showed similar pattern to the obtained during desert dust events. Therefore, AAE^{is} and SAE^{is} from in-situ measurements are not a useful tool for confirming desert dust

425 events of low and medium intensity in our urban station.

426 We performed a non-parametric test (Kolmogorov-Smirnov) in order to compare
427 the optical parameters obtained during desert dust and dust-free conditions (Table 2). This
428 test shows that there was significant differences between SAE^{col} and AAE^{col} obtained
429 during desert dust events and those observed during dust-free conditions. Similar result
430 was found for SAE^{is} at surface. However, this test revealed that no significant difference
431 was found for AAE^{is} between desert dust and free-dust conditions. In this sense, it should
432 be interesting to analyze extreme dust cases in order to find clear differences in these
433 optical parameters between dust and free-dust conditions. Extreme events will be
434 analyzed and discussed in section 4.3.

435 **4.2. Relationships between single scattering albedo and Fine mode Fraction of AOD**
436 **during desert dust events**

437 According to the values of ω^{col} and ω^{is} shown in the previous sections there are
438 evidences of the significant contribution of absorbing fine particles in atmospheric column
439 and at surface during both desert dust and dust-free conditions. In order to quantify the
440 fine mode particles contribution during desert dust events and its relationship with ω^{col} and
441 ω^{is} we used the Fine Mode Fraction (FMF) of the AOD provided by AERONET. In this

442 section, the relationship between single scattering albedo and Fine Mode Fraction (FMF)
443 during dusty conditions is evaluated.

444 The single scattering albedo as a function of FMF during dust events is shown in
445 Figure 5. The error bars are the standard deviations. The single scattering albedo was
446 averaged for each range bin of the Fine Mode Fraction considered. The mean values of
447 SAE^{col} and AAE^{col} and their corresponding standard deviations for each FMF bin are
448 included in Figure 5. During dusty conditions, FMF was in 0.2-0.3 bin in 51% of cases.
449 From Figure 5, it is clear that ω^{col} increased with wavelength. In addition, this increase with
450 wavelength is stronger when FMF decreases. This is the typical pattern of ω^{col} in situations
451 dominated by desert dust with strong absorption in the ultraviolet and less absorption in
452 the infrared spectral region. As FMF increases the spectral dependence of ω^{col} in the 670-
453 1020 nm spectral range becomes practically neutral and even ω^{col} slightly decreases with
454 increasing wavelength for FMF > 0.4. It is noticed that when mineral coarse particles were
455 dominating, FMF in range [0.1-0.2], AAE^{col} showed higher values (1.82) with strongly
456 absorption in shorter wavelengths. Therefore, the increase in the FMF was associated with
457 an increase in anthropogenic absorbing aerosol (black carbon which is absorbent in the
458 entire spectral range).

4.3 Special Event

A case study of an intense desert dust event is analysed in this section in more detail. According to the CALIMA database, the event lasted from 11 to 22 October 2008. Figure 6 shows the time series of SAE^{is}, SAE^{col}, σ_{sp} and AOD_{scat} for the period 9-31 October. The CIMEL data are instantaneous values whilst the nephelometer data are 5-min average values. As can be observed in Figure 6, SAE^{is} and SAE^{col} had values close to 0 during the period 11-14 October, evidencing a predominance of coarse particles both at surface level and in the atmospheric column. During this period, the σ_{sp} and AOD_{scat} parameters increased considerably reaching values up to 700 Mm^{-1} and 1, respectively. After this period, σ_{sp} and AOD_{scat} decreased and the SAE^{is} and SAE^{col} increased, denoting an increase in the contribution of fine particles. However, SAE^{col} remained below 1 until 24 October whilst SAE^{is} was more variable reaching values up to 2. These differences between in situ and column measurements can be ascribed to the variations in the vertical distribution of dust particles as suggested by the BSC-DREAM modelled dust concentrations (http://www.bsc.es/earth-sciences/mineral-dust-forecast-system/bsc-dream8b-forecast/north-africa-europe-and-middle-ea-0) and to changes in local emissions. At surface level, σ_{sp} showed two maxima per the day in coincidence with traffic rush hours

476 (Lyamani et al., 2010) which was not observed in the AOD_{scat} measurements. The dust
477 intrusion was more intense during the period 11-15, especially at ground level (Figure 6).
478 The spectral dependence of the optical properties both measured with in-situ
479 instrumentation and sun-photometer during the intense dust event days at surface and on
480 30 October have been analysed. This last day has been included in order to compare the
481 aerosol properties obtained during dust-free conditions with those observed during desert
482 dust events. Furthermore, 24-hours chemical composition in PM_{10} fraction for 13, 14, 22
483 and 30 October and in PM_1 for 30 October has been used to support the interpretation of
484 the results. Information about the sampling procedure and the chemical analysis can be
485 found in Titos et al. (2012). Figure 7 shows the chemical speciation of PM_{10} samples
486 collected on 13, 14, 22 and 30 October and the PM_1 sample collected on 30 October. In
487 addition, the percentage of Fe, Elemental Carbon (EC) and Organic Carbon (OC) in each
488 sample is shown in this figure. PM_{10} mass concentration was close to 90 $\mu g/m^3$ on 13
489 October. The mineral matter (ΣAl_2O_3, SiO_2, CO_3^{2-}, Ca, Fe, Mg, K) contributed around 70%
490 to PM_{10} on 13 October, 44% on 14 October, 25% and 21% on 22 and 30 October,
491 respectively. On 30 October, the ratio PM_1/PM_{10} was 0.63 denoting a clear predominance
492 of fine particles. Thus, considering the chemical speciation in PM_{10} and PM_1 on 30 October

493 it seems that this day was not affected by desert dust and could be considered as dust-
494 free conditions.

495 Figure 8 shows the mean values of $AOD_{scat}(\lambda)$ and $\sigma_{sp}(\lambda)$ for 11-13, 14 and 30
496 October. The error bars are the corresponding standard deviations. The mean values were
497 calculated from the coincident instantaneous values. The mean AAE^{col} and SAE^{col} values
498 and their corresponding standard deviations are included in Figure 8. The SAE^{col}
499 presented values close to zero for the period 11-13 and 14, and increased considerably on
500 30 October. A similar behaviour was observed from in-situ measurements, although the
501 increase in the SAE^{is} from the period 11-13 to 14 October was much pronounced
502 indicating a strong decrease in dust intensity at ground level on 14 October. In fact, the
503 columnar aerosol load for 11-13 and 14 was very similar but at ground level there was a
504 strong decrease in the scattering coefficient on 14 October (see Figure 6). It is important
505 to note that the differences in SAE^{col} and SAE^{is} obtained in dust-free and dust conditions
506 are more pronounced for this special event.

507 The AAE^{col} and AAE^{is}(Figure 9) were higher for the period 11-13 compared to 30
508 October (dust free conditions). Thus, during the dust event the surface absorption
509 coefficient and the absorption optical depth experienced an enhancement in the shorter

510 wavelengths. Mineral dust contributes to light absorption in the ultraviolet and blue spectral
511 regions yielding to AAE values greater than 1 (Kirchstetter et al., 2004). Iron oxides
512 (primarily hematite and goethite) are major components that affect the ability of dust to
513 absorb sunlight (Arimoto et al., 2002). Indeed, the contribution of Fe to the PM_{10} mass
514 concentration was higher during the dust event (3.5% and 2.5% on 13 and 14 October)
515 compared to dust-free conditions (1.3% on 30 October). In addition, the contribution of OC
516 and EC to the PM_{10} mass concentration was lower on 13 October suggesting that the
517 observed absorption enhancement in the shorter wavelengths may be caused by Fe.
518 AAE^{is} values were of2.5±0.2 on 12 October and 1.12±0.03 on 30 October and the AAE^{col}
519 values were of 1.8±0.2 on 11-13 October and 1.16±0.09 on 30 October. A higher
520 absorption at shorter wavelengths during dust conditions can be also observed in the
521 aerosol single scattering albedo (Figure 10). This parameter increased with wavelength
522 during the dust event. This increase was more noticeable during the period 11-13 in
523 column than at ground level. The $\omega(\lambda)$ spectral dependence on 30 October was opposite to
524 the obtained during the dust event. This parameter had values close to 1 during the dust
525 event, both in column and at ground level, and much lower values on 30 October.

526 **5. CONCLUSIONS**

527 In situ and passive remote sensing instruments were used to measure aerosol optical
528 properties at surface and in atmospheric column during desert dust events and dust-free
529 conditions at Granada. The scattering and absorption Angström exponents as well as the
530 single scattering albedo obtained in these conditions during 2008-2010 were evaluated in
531 both at the surface and in atmospheric column.
532 The mean value of scattering Angström exponent in atmospheric column obtained during
533 dusty days was of 0.5±0.2, indicating a significant contribution of large particles to the total
534 columnar aerosol load during desert dust events observed over Granada during 2008-
535 2010. However, SAE^{is} mean value obtained at surface during dusty conditions was of
536 1.3±0.6, indicating higher contribution of coarse particles at high atmospheric level than at
537 ground level. This result is in agreement with previous studies performed at Granada,
538 showing that usually desert dust is transported at high altitude over Granada. Although the
539 single scattering albedo in the atmospheric column and at surface increased with
540 wavelength during dusty conditions, this parameter showed lower values than those
541 reported for pure desert dust cases. In addition, it is noticed that the mean value of
542 absorption Angström exponent in the atmospheric column was of 1.5±0.2, indicating a
543 mixture of desert dust and black carbon particles as dominant absorbers during dust

intrusions over Granada. On the other hand, mean AAE^{is} value obtained during dusty days was of 1.3±0.2 which was similar to that obtained in dust-free conditions (1.4±0.3), probably due to the small dust (iron oxides) contribution at the surface during the majority of analyzed dust events. Indeed, a non-parametric test (Kolmogorov-Smirnov) revealed that the AAE^{is} difference between desert dust and free-dust conditions is not statistically significant. The results suggest that AAE^{is} parameter should not be used alone to identify dust particles during low-moderate intense dust intrusions in urban locations as Granada with significant anthropogenic aerosol presence without the use of other information (e.g., aerosol size). A dust extreme event was analyzed in order to retrieve optical parameters during situation dominated by dust particles. The values of SAE^{col} (AAE^{col}) and SAE^{is} (AAE^{is}) were in agreement with the values showed above for the period 2008-2010, although the differences between dust-free and dust conditions are more noticeable for the special event.

Acknowledgments— This work was supported by the Andalusia Regional Government through projects P12-RNM-2409 and P10-RNM-6299, by the Spanish Ministry of Science and Technology through projects CGL2010-18782, CSD2007-00067, CGL2011-29921-C02-01 and CGL2011-13580-E/CLI; and by EU through ACTRIS project (EU INFRA-2010-1.1.16-262254). Manuel Antón thanks *the* Ministerio de Ciencia e Innovación and Fondo Social Europeo for the award of a

postdoctoral grant (Ramón y Cajal). CIMEL Calibration was performed at the AERONET-EUROPE calibration center, supported by ACTRIS (European Union Seventh Framework Program (FP7/2007-2013) under grant agreement no. 262254. The authors thankfully acknowledge the computer resources, technical expertise and assistance provided by the Barcelona Supercomputing Center for the BSC-DREAM8b model dust data (*http://www.bsc.es/earth-sciences/mineral-dust-forecast-system/bsc-dream8b-forecast*).

REFERENCES

Anderson, T.L.,Wu, Y., Chu, D.A., Schmid, B., Redemann, J., Dubovik, O., 2005. Testing the MODIS satellite retrieval of aerosol fine-mode fraction. Journal of Geophysical Research. doi:10.1029/2005JD005978.Bergstrom, R.W., Pilewskie, P., Russell, P.B., Redemann, J., Bond, T.C., Quinn, P.K., Sierau, B., 2007. Spectral absorption properties of atmospheric aerosols. Atmos. Chem. Phys., 7, 5937-5943.

Anderson, T. L. and Ogren, J. A., 1998. Determining aerosol radiative properties using the TSI 3563 integrating nephelometer. Aerosol. Sci. Tech., 29, 57–69.

Andreae, M.O., Schmid, O., Yang, H., Chand, D., Zhen Yu, J., Zeng, L.-M., Zhang, Y.-H., 2008. Optical properties and chemical composition of the atmospheric aerosol in urban Guangzhou, China. Atmos. Environ., 42, 6335-6350.

Alados-Arboledas, L., A. Alcántara, F.J. Olmo, J.A. Martínez-Lozano, V. Estellés, V. Cachorro, A.M. Silva, H. Horvath, M. Gangl, A. Díaz, M. Pujadas, J. Lorente, A. Labajo, M. Sorribas, and G. Pavese, 2008. Aerosol columnar properties retrieved from CIMEL radiometers during VELETA 2002, Atmos. Environ., 42, 2654–2667.

Angström, A.: On the atmospheric transmission of sun radiation and on dust in the air, Geograf. Ann. Deut., 11, 156–166, 1929.

IPCC (Intergovernmental panel on Climate Change), 2007. In: Solomon, S., Qin, D., Manning, M., Chen, Z., Marquis, M., Averyt, K.B., Tignor M.M.B., Miller, H.L. (Eds.), Climate

589 Change 2007: the physical science basis. Cambridge Univ. Press, Cambridge, UK, and
590 New York, USA.
591 Bergstrom, R.W., Pilewskie, P., Pommier, J., Rabbette, M., Russell, P.B., Schmid, B., Redemann,
592 J., Higurashi, A., Nakajima, T., Quinn, P.K., 2004. Spectral absorption of solar radiation
593 by aerosols during ACE-Asia. J. Geophys. Res., 109, D19S15,
594 doi:10.1029/2003JD004467.
595 Bergstrom, R.W., Pilewskie, P., Russell, P.B., Redemann, J., Bond, T.C., Quinn, P.K., Sierau, B.,
596 2007. Spectral absorption properties of atmospheric aerosols. Atmos. Chem. Phys., 7,
597 5937-5943.
598 Bergstrom, R.W., Schmidt, K.S., Coddington, O., Pilewskie, P., Guan, H., Livingston, J.M.,
599 Redemann, J., Russell, P.B., 2010. Aerosol spectral absorption in the Mexico City area:
600 results from airborne measurements during MILAGRO/INTEX B. Atmos. Chem. Phys.,
601 10, 6333-6343.
602 Bodhaine, B.A., 1995. Aerosol absorption measurements at Barrow, Mauna Loa and the south pole.
603 J. Geophys. Res., 100, 8967-8975.
604 Bond, T. C., Anderson, T. L. and Campbell, D., 1999. Calibration and intercomparison of filter-
605 based measurements of visible light absorption by aerosols. Aerosol Sci. Technol., 30,
606 582– 600.
607 Cachorro, V.E., C. Toledano, N. Prats, M. Sorribas, S. Mogo, A. Berjón, B. Torres, R. Rodrigo, J.
608 de la Rosa, and A. M. De Frutos. , 2008. The strongest desert dust intrusion mixed with
609 smoke over the Iberian Peninsula registered with Sun photometry. J. Geophys. Res., 113,
610 D14S04, doi:10.1029/2007JD009582.
611 Charlson, R., Schwartz, 5 S., Hales, J., Cess, R., Coakley, J., Hansen, J., and Hofman, D.: Climate
612 forcing by anthropogenic aerosols, Science, 255, 423–430,
613 doi:10.1126/science.255.5043.423, 1992.
614 Clarke, A.D., Shinozuka, Y., Kapustin, V.N., Howell, S., Huebert, B., Doherty, S., Anderson, T.,

615 Covert, D., Anderson, J., Hua, X., Moore, K.G., McNaughton, C., Carmichael, G.,
616 Weber, R., 2004. Size distributions and mixtures of dust and black carbon aerosol in
617 Asian outflow: Physiochemistry and optical properties. J. Geophys. Res., 109, D15S09,
618 doi:10.1029/2003JD004378.
619 Collaud Coen, M., Weingartner, E., Schaub, D., Hueglin, C., Corrigan, C., Henning, S.,
620 Schwikowski, M., Baltensperger, U., 2004. Saharan dust events at the Jungfraujoch:
621 detection by wavelength dependence of the single scattering albedo and first climatology
622 análisis, Atmos.Chem.Phys., 4, 1–16.
623 Córdoba-Jabonero, C., Sorríbas, M., Guerrero-Rascado, J.L., Adame, J. A., Hernández, Y.,
624 Lyamani, H., Cachorro, V., Gil, M., Alados-Arboledas, L., Cuevas, E., and de la Morena,
625 B., 2011. Synergetic monitoring of Saharan dust plumes and potential impact on surface:
626 a case study of dust transport from Canary Islands to Iberian Peninsula.
627 Atmos.Chem.Phys., 11, 3067-3091.
628 Costabile, F., Barnaba, F., Angelini, F., and Gobbi, G. P.: Identification of key aerosol populations
629 through their size and composition resolved spectral scattering and absorption, Atmos.
630 Chem. Phys., 13, 2455-2470, doi:10.5194/acp-13-2455-2013, 2013.
631 Draxler, R.R., Stunder, B., Rolph, G., Taylor, A., 2009. HYSPLIT_4 User's Guide. NOAA Air
632 Resources Laboratory.
633 Dubovik, O., Holben, B. N., Kaufman, Y. J., Yamasoe, M., Smirnov, A., Tanre, D. and Slutsker,
634 I., 1998. Single-scattering albedo of smoke retrieved from the sky radiance and solar
635 transmittance measured from ground. J. Geophys. Res., 103, 31 903–31 924.
636 Dubovik, O., Sinyuk, A., Lapyonok, T., Holben, B.N., Mishchenko, M., Yang, P., Eck, T.F.,
637 Volten, H., Muñoz, O., Veihelmann, B., van der Zande, W.J., Leon, J.F., Sorokin, M.,
638 Slutsker, I., 2006. Application of spheroid models to account for aerosol particle
639 nonsphericity in remote sensing of desert dust. J. Geophys. Res., 111, D11208,
640 doi:10.1029/2005JD006619, 2006.

641 Dubovik, O., and King M. D., 2000. A flexible inversion algorithm for retrieval of aerosol optical
642 properties from sun and sky radiance measurements, J. Geophys. Res., 105, 20,673–
643 20,696.
644 Eck, T.F., Holben, B.N., Sinyuk, A., Pinker, R.T., Goloub, P., Chen, H., Chatenet, B., Li, Z., Singh,
645 R.P., Tripathi, S.N., Reid, J.S., Giles, D.M., Dubovik, O., O'Neill, N.T., Smirnov, A.,
646 Wang, P., Xia, X. , 2010. Climatological aspects of the optical properties of fine/coarse
647 mode aerosol mixtures, J. Geophys. Res., 115, D19205, doi: 10.1029/2010JD014002.
648 Fialho, P., Hansen, A.D.A., Honrath, R.E., 2005. Absorption coefficients by aerosols in remote
649 areas: a new approach to decouple dust and black carbon absorption coefficients using
650 seven-wavelength Aethalometer data. J. Aerosol. Sci., 36, 267-282.
651 Flowers, B.A., Dubey, M.K., Mazzoleni, C., Stone, E.A., Schauer, J.J., Kim, S.W., Yoon, S.C.,
652 2010. Optical-chemical-microphysical relationships and closure studies for mixed
653 carbonaceous aerosols observed at Jeju Island; 3-laser photoacoustic spectrometer,
654 particle sizing, and filter analysis. Atmos. Chem. Phys., 10, 10387-10398.
655 Guerrero-Rascado, J. L., F.J. Olmo, I. Avilés-Rodríguez, F., Navas-Guzmán, D. Pérez-Ramírez, H.
656 Lyamani, and L. Alados Arboledas, 2009. Extreme Saharan dust event over the southern
657 Iberian Peninsula in september 2007: active and passive remote sensing from surface and
658 satellite, Atmos. Chem. Phys., 9, 8453–8469.
659 Höller, R., Ito, K., Tohno, S., kasahara, M., 2003. Wavelength-dependent aerosol single-scattering
660 albedo: measurements and model calculations for a coastal site near the Sea of Japan
661 during ACE-Asia. Journal of Geophysical Research 108 (D23), 8648.
662 Holben, B.N., Eck, T.F., Slutsker, I., Tanre, D., Buis, J.P., Setzer, A., Vermote, E., Reagan, J.A.,
663 Kaufman, Y.J., Nakajima, T., Lavenu, F., Jankowiak, I., Smirnov, A., 1998. AERONET -
664 A federated instrument network and data archive for aerosol characterization. Remote
665 Sens. Environ., 66, 1-16.
666 Kaskaoutis, D. G. and Kambezidis, H. D.: Comparison of the Angtröm parameters retrieval in

667 different spectral ranges with the use of different techniques, Meteorol. Atmos. Phys., 99,
668 233–246, doi:10.1007/s00703-007-0279-y, 2008.
669 Kim, S.-W., Yoon, S.-C., Jefferson, A., Ogren, J.A., Dutton, E.G., Won, J.-G., Ghim, Y.S., Lee, B.-
670 I., Han, J.-S., 2005. Aerosol optical, chemical and physical properties at Gosan, Korea
671 during Asian dust and pollution episodes in 2001. Atmos. Environ., 39, 39-50.
672 Kim, D., Chin, M. Yu, H., Eck, T. F., Sinyuk, A., Smirnov, A., and Holben, B. N. 2011. Dust
673 optical properties over North Africa and Arabian Peninsula derived from the AERONET
674 dataset. Atmos. Chem. Phys., 11, 10733-10741.
675 Knippertz, P., et al. (2009), Dust mobilization and transport in the northern Sahara during SAMUM
676 2006—A meteorological overview, Tellus, Ser. B, 61, 12–31.
677 Lack, D. A. and Cappa, C. D.: Impact of brown and clear carbon on light absorption enhancement,
678 single scatter albedo and absorption wavelength dependence of black carbon, Atmos.
679 Chem. Phys. Discuss., 10, 785–819, 2010, http://www.atmos-chem-phys-
680 discuss.net/10/785/2010/.
681 Lee, S., Yoon, S.-C., Kim, S.-W., Kim, Y.P., Ghim, Y.S., Kim, J.-H., Kang, C.-H., Kim, Y.J.,
682 Chang, L.-S., Lee, S.-J., 2012. Spectral dependency of light scattering/absorption and
683 hygroscopicity of pollution and dust aerosols in Northeast Asia. Atmos. Environ., 50,
684 246-254.
685 Lyamani, H., Olmo, F. J., Alcántara, A. and Alados-Arboledas, L., 2006. Atmospheric aerosols
686 during the 2003 heat wave in southeastern Spain II: Microphysical columnar properties
687 and radiative forcing. Atmos. Environ., 40, 6465-6476.
688 Lyamani, H., Olmo, F.J., Alados-Arboledas, L., 2010. Physical and optical properties of aerosols
689 over an urban location in Spain: seasonal and diurnal variability. Atmos. Chem. Phys.,
690 10, 239-254.
691 Perrone, M.R., Bergamo, A., 2011. Direct radiative forcing during Sahara dust intrusions at a site in
692 the Central Mediterranean: Anthropogenic particle contribution. Atmos. Res.

693 doi:10.1016/jatmosres.2011.05.011.
694 Quirantes, A., Olmo, F. J., Lyamani, H., and Alados-Arboledas, L., 2008. Correction factors for a
695 total scatter/backscatter nephelometer. J. Quant. Spectrosc. Ra., 109, 1496–1503.
696 Rizzo, L. V., Correia, A. L., Artaxo, P., Procopio, A. S., and Andreae, M. O., 2011. Spectral
697 dependence of aerosol light absorption over the Amazon Basin, Atmos. Chem. Phys., 11,
698 8899–8912, doi:10.5194/acp-11-8899-2011.
699 Russell, P.B., Bergstrom, R.W., Shinozuka, Y., Clarke, A.D., DeCarlo, P.F., Jimenez, J.L.,
700 Livingston, J.M., Redemann, J., Dubovik, O., Strawa, A., 2010. Absorption Angstrom
701 Exponent in AERONET and related data as an indicator of aerosol composition. Atmos.
702 Chem. Phys., 10, 1155-1169.
703 Schladitz, A. M¨uller, T., Massling, A., Kaaden, N., Kandler, K., Ebert, M., Weinbruch, S.,
704 Deutscher, C. and Wiedensohler, A., 2009. In situ measurements of optical properties at
705 Tinfou (Morocco) during the Saharan Mineral Dust Experiment SAMUM 2006. Tellus
706 61B, 64–78.
707 Saha, A., Mallet, M., Roger, J.C., Dubuisson, P., Piazzola, J., Despiau, S., 2008. One year
708 measurements of aerosol optical properties over an urban coastal site: Effect on local
709 direct radiative forcing. Atmos. Res., 90, 195-202.
710 Smirnov, A., Holben, B.N., Eck, T.F., Dubovik, O., Slutsker, I., 2000. Cloudscreening and quality
711 control algorithms for the AERONET database. Remote. Sens. Environ. 73, 337–349.
712 Sokolik, I.N., Toon, O.B., 1999. Incorporation of mineralogical composition into models of the
713 radiative properties of mineral aerosol from UV to IR wavelengths. J. Geophys. Res.,
714 104, 9423-9444.
715 Soni, K., Singh, S., Bano, T., Tanwar, R.S., Nath, S., Arya, B.C., 2010. Variations in single
716 scattering albedo and Angstrom absorption exponent during different seasons at Delhi,
717 India. Atmos. Environ., 44, 4355-4363.
718 Su, L., Toon, O.B., 2011. Saharan and Asian dust: similarities and differences determined by

719 CALIPSO, AERONET, and a coupled climate-aerosol microphysical model. Atmos.
720 Chem. Phys., 11, 3263-3280.
721 Schwartz, S.: The Whitehouse effect – Shortwave radiative forcing of climate by anthropogenic
722 aerosols: an overview, J. Aerosol. Sci., 27, 359–382, doi:10.1016/0021-8502(95)00533-
723 1, 1996.
724 Tesche, M., Ansmann, A., Müller, D., Althausen, D., Mattis, I., Heese, B., Freudenthaler, V.,
725 Wiegner, M., Esselborn, M., Pisani, G., Knippertz, P., 2009. Vertical profiling of Saharan
726 dust with Raman lidars and airborne HSRL in southern Morocco during SAMUM.
727 Tellus 61B, 144-164.
728 Titos G, Foyo-Moreno I, Lyamani H, Querol X, Alastuey A, Alados-Arboledas L.: Optical
729 properties and chemical composition of aerosol particles at an urban location: An
730 estimation of the aerosol mass scattering and absorption efficiencies, J. Geophys. Res.,
731 117, D04206, doi:10.1029/2011JD016671, 2012.
732 Titos, G., Lyamani, H., Cazorla, A., Sorribas, M., Foyo-Moreno, I., Wiedensohler, A., and Alados-
733 Arboledas, L.: Study of the relative humidity dependence of aerosol light-scattering
734 in southern Spain, Tellus B, 66, 24536, doi:10.3402/tellusb.v66.24536, 2014.
735 Toledano, C., Wiegner, M., Gross, S., Freudenthaler, V., Gasteiger, J., Mueller, D., Mueller, T.,
736 Schladitz, A., Weinzierl, B., Torres, B., O'Neill, N.T., 2011. Optical properties of aerosol
737 mixtures derived from sun-sky radiometry during SAMUM-2. Tellus 63B, 635-648.
738 Valenzuela, A., Olmo, F.J., Lyamani, H., Antón, M., Quirantes, A., Alados-Arboledas, L., 2012a.
739 Analysis of the desert dust radiative properties over Granada using principal plane sky
740 radiances and spheroids retrieval procedure. Atmos. Res., 104-105, 292–301.
741 Valenzuela, A., Olmo, F.J., Lyamani, H., Antón, M., Quirantes, A., Alados-Arboledas, L., 2012b.
742 Classification of aerosol radiative properties during African desert dust intrusions over
743 southeastern Spain by sector origins and cluster analysis, J. Geophys. Res., 117, D06214,
744 doi:10.1029/2011JD016885, 2012a.

745 Valenzuela, A., Olmo, F.J., Lyamani, H., Antón, M., Quirantes, A., Alados-Arboledas, L., 2012c.
746 Aerosol radiative forcing during African desert dust intrusions (2005-2010) over
747 Southeaster Spain. Atmos. Chem. Phys., 12, 10331–10351, 2012b.
748 Yang, M., Howell, S. G., Zhuang, J., and Huebert, B. J., 2009. Attribution of aerosol light
749 absorption to black carbon, brown carbon, and dust in China – interpretations of
750 atmospheric measurements during EAST-AIRE, Atmos. Chem. Phys., 9, 2035–2050,
751 doi:10.5194/acp-9-2035-2009.
752
753
754 FIGURES
755
756 **Figure 1:** Single scattering albedo and its standard deviation during desert dust events (in
757 atmospheric column with full circle symbol, in surface with full start symbol) and during
758 dust-free conditions (in atmospheric column with unfilled circle symbol, in surface with
759 unfilled start symbol).
760 **Figure 2:** a) Aerosol scattering optical depths, SAE^{col}, and their standard deviations in
761 atmospheric column during desert dust events (full bars) and dust-free conditions (hatched
762 bars) and b) aerosol scattering coefficients, SAE^{is}, and their standard deviations at the
763 surface during desert dust events (full bars) and dust-free conditions (hatched bars).
764 **Figure 3:** a) Aerosol absorption optical depths, AAE^{col}, and their standard deviations in

765 atmospheric column during desert dust events (full bars) and dust-free conditions (hatched
766 bars) and b) aerosol absorption coefficients, AAE^{is}, and their standard deviations at the
767 surface during desert dust events (full bars) and dust-free conditions (hatched bars).
768 **Figure 4:** Relative frequency of scattering and absorption Angstrom exponents during
769 desert dust events in atmospheric column (a and b) and at the surface (e and f), and
770 during dust-free conditions in atmospheric column (c and d) and at the surface (g and h).
771 **Figure 5:** Single scattering albedo averaged for different Fine Mode Fraction (FMF) bins
772 during desert dust introsions over Granada. The error bars are the standard deviations.
773 SAE^{col} and AAE^{col} averaged for each FMF bin and the corresponding standard deviations
774 are also included in the Figure. .
775 **Figure 6:** Aerosol light scattering coefficient at 450, 550 and 700 nm, $AOD_{scat}(\lambda)$,
776 SAE^{col}(440-1020), and SAE^{is}(450-700) obtained over Granada during the period 9-31
777 October 2008.
778 **Figure 7:** Mass concentration expressed in $\mu g/m^3$ of the major constituents in PM10 for the
779 sampling days 13, 14, 22 and 30th of October and in PM1 for the 30th of October. The ratio
780 OC/EC is also shown (right axe) and the percentage of Fe and EC during each sampling
781 day is included.

782 **Figure 8:** Aerosol scattering optical depth and its standard deviation in atmospheric column
783 (left panel) and surface aerosol scattering coefficient and its standard deviation (right
784 panel), for the periods 11-13, 14 and 30th of October 2008.

785 **Figure 9:** Aerosol absorption optical depth and its standard deviation in atmospheric
786 column (left panel) and surface aerosol absorption coefficient and its standard deviation
787 (right panel), for the periods 11-13, 14 and 30th of October 2008.

788 **Figure 10:** Single scattering albedo and its standard deviation in atmospheric column (left
789 panel) and measured with in situ instrumentation at the surface (right panel), for the
790 periods 11-13, 14 and 30th of October 2008.

791

792

793

794

TABLES

Table 1: Comparison of aerosol optical properties with those obtained in other locations.

Authors	Aerosol type	$SAE^{col}(*)$	$SAE^{is}(*)$	$AAE^{col}(*)$	$AAE^{is}(*)$	$\omega^{col}(\lambda)(\#)$	$\omega^{is}(\lambda)$ (#)	Location
Kim et al. (2011)	Dust					0.90-0.94 at 440		Tamanrasset, Algeria
Dubovik et al. (2002b)	Dust					0.92 and 0.97 at 440 and 1020		Solar Village, Saudi Arabia
Perrone and Bergamo, (2011)	Dust					0.87-0.95 at 550		Lecce, Italy
Lyamani et al. (2006b)	Urban-Industrial					0.91 and 0.85 at 440 and 1020		Granada, Spain
Kim et al. (2005)	Dust	0.38±0.03 at 412-862	0.66±0.03 at 450-700				0.91 at 550	Gosan, Korea
Kim et al. (2005)	Urban-Industrial	1.3±0.03 at 412-862	1.4±0.03 at 450-700				0.91 at 550	Gosan, Korea
Yang et al. (2009)	Dust		0.59±0.03 at 450-700		1.89±0.03 at 470-660		0.90 at 550	Beijing, China
Yang et al. (2009)	Urban-Industrial		1.39±0.03 at 450-700		1.5±0.03 at 470-660		0.80 at 550	Beijing, China
Soni et al. (2010)	Urban-Industrial						0.70 at 550	Delhi, India
Saha et al. (2008)	Urban-Industrial						0.73-0.78 at 525	Toulon, France
Andreae et al. (2008)	Urban-Industrial						0.83 at 540	Guangzhou, China
This study	Dust	0.5±0.03 at 440-1020	1.1±0.03 at 450-700	1.5±0.03 at 440-1020	1.3±0.03 at 467-650	0.89 and 0.96 at 440 and 1020	0.74 and 0.76 at 467 and 650	Granada, Spain
This study	Free-dust	1.2±0.03 at 440-1020	1.6±0.03 at 450-700	0.9±0.03 at 440-1020	1.4±0.03 at 467-650	0.90 and 0.86 at 440 and 1020	0.62 and 0.61 at 467 and 650	Granada, Spain

816 (∗) Spectral range used to retrieve the SAE^{col}, SAE^{is}, AAE^{col} and AAE^{is} parameters in nm, (#) Wavelength in nm

Table 2: The p values of the Kolmogorov-Smirnov statistical test applied to SAE and AAE retrieved in the atmospheric column and at surface for each pair of data set (Desert dust and Dust-Free conditions). The p values of the diagonal, for each pair of data, indicate statistical significant. Values of $p < 0.05$ indicate statistical significant differences between the means at the 95% confidence level. The subscript "DD" and "DF" mean Desert dust and Dust-Free conditions, respectively.

	SAE^{col}_{DD}	AAE^{col}_{DD}	SAE^{is}_{DD}	AAE^{is}_{DD}
SAE^{col}_{DF}	0.093	---	---	---
AAE^{col}_{DF}	---	0.147	---	---
SAE^{is}_{DF}	---	---	0.141	---
AAE^{is}_{DF}	---	---	---	**0.017**

FIGURES

Figure 1

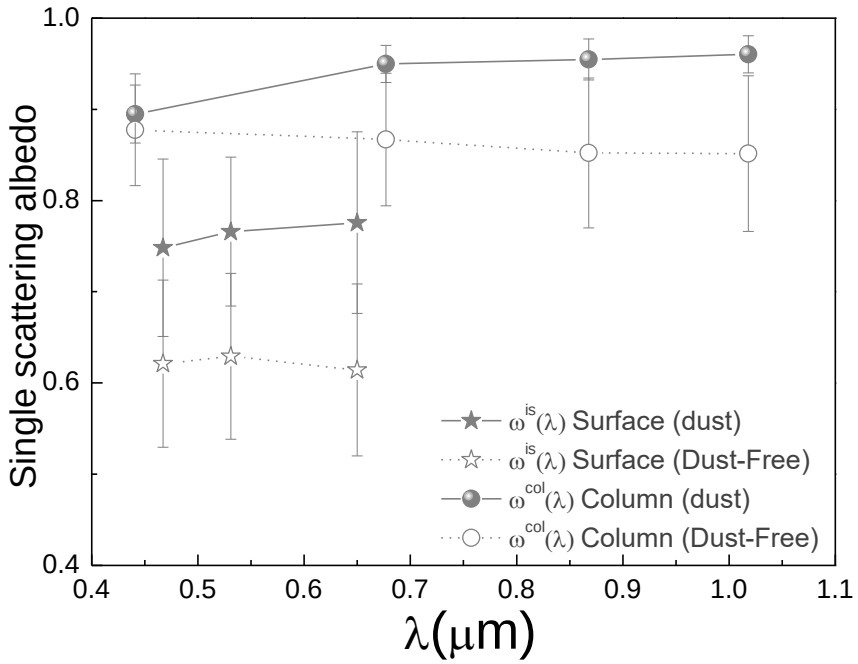

Figure 2

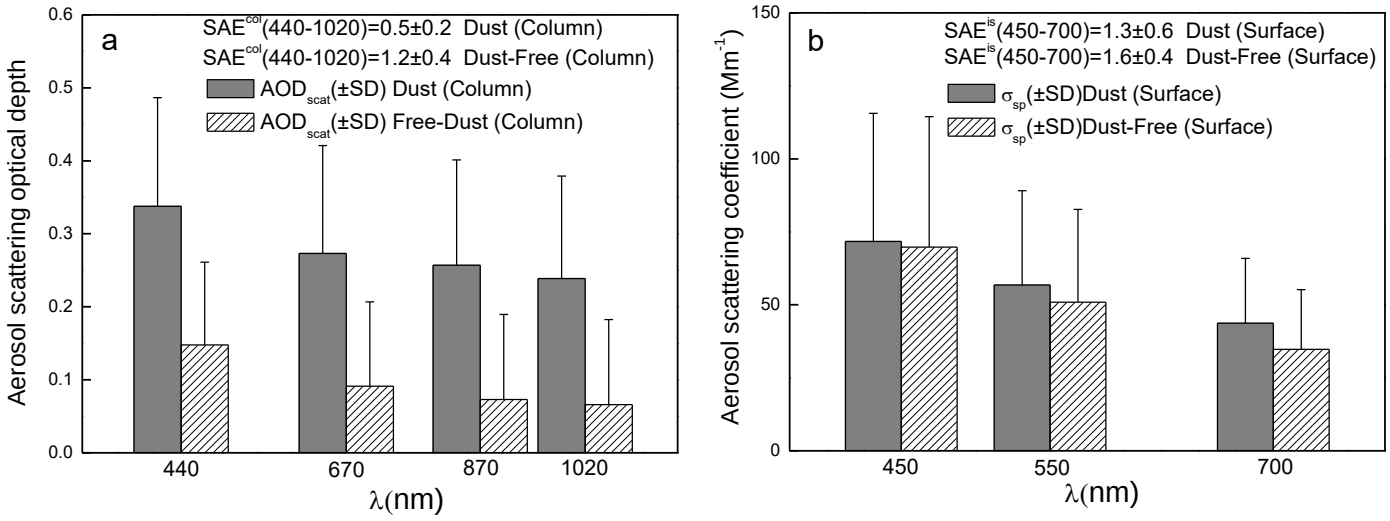
a
SAE^col(440-1020)=0.5±0.2 Dust (Column)
SAE^col(440-1020)=1.2±0.4 Dust-Free (Column)
AOD_scat(±SD) Dust (Column)
AOD_scat(±SD) Free-Dust (Column)
Aerosol scattering optical depth
0.0
0.1
0.2
0.3
0.4
0.5
0.6
440
670
870
1020
λ(nm)
b
SAE^is(450-700)=1.3±0.6 Dust (Surface)
SAE^is(450-700)=1.6±0.4 Dust-Free (Surface)
σ_sp(±SD)Dust (Surface)
σ_sp(±SD)Dust-Free (Surface)
Aerosol scattering coefficient (Mm^-1)
0
50
100
150
450
550
700
λ(nm)

Figure 3

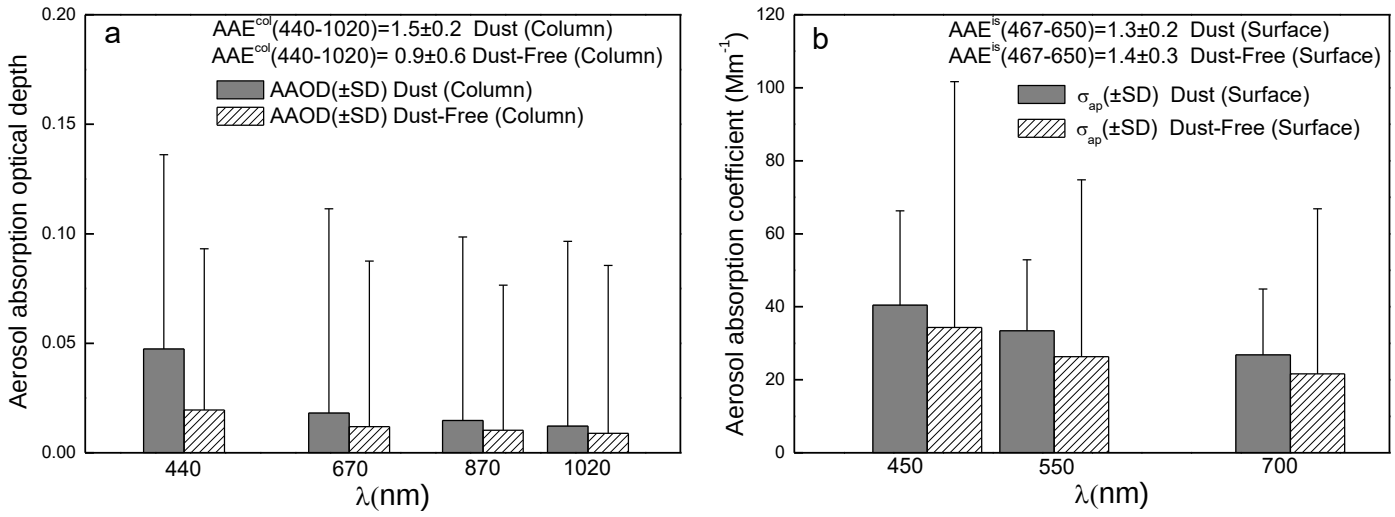
a
AAE^col(440-1020)=1.5±0.2 Dust (Column)
AAE^col(440-1020)= 0.9±0.6 Dust-Free (Column)
AAOD(±SD) Dust (Column)
AAOD(±SD) Dust-Free (Column)
Aerosol absorption optical depth
0.20
0.15
0.10
0.05
0.00
440
670
870
1020
λ(nm)
b
AAE^ls(467-650)=1.3±0.2 Dust (Surface)
AAE^ls(467-650)=1.4±0.3 Dust-Free (Surface)
σap(±SD) Dust (Surface)
σap(±SD) Dust-Free (Surface)
Aerosol absorption coefficient (Mm-1)
120
100
80
60
40
20
0
450
550
700
λ(nm)

Figure 4

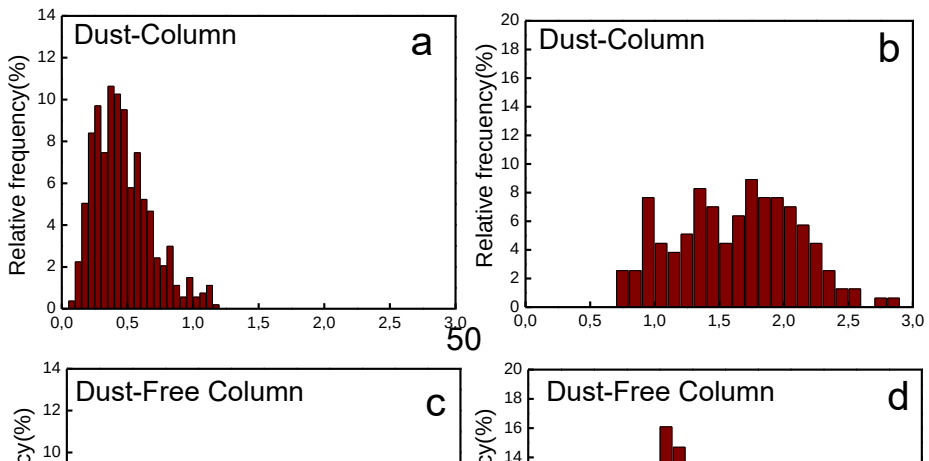
Dust-Column
a
Relative frequency(%)
Dust-Column
b
Relative frecuency(%)
Dust-Free Column
c
Dust-Free Column
d

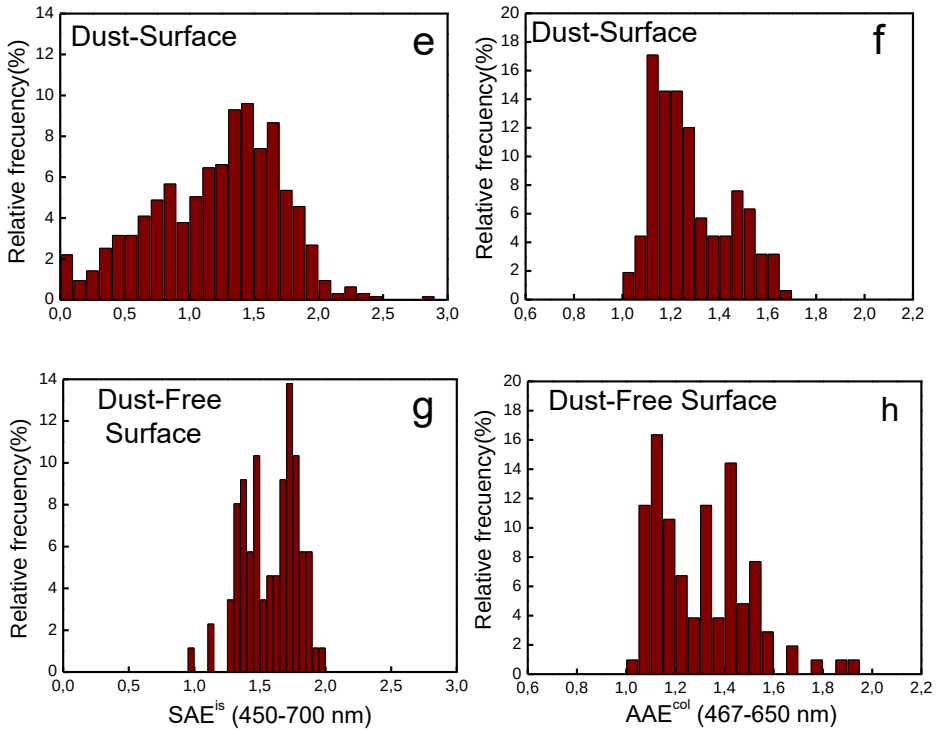
Dust-Surface
e
Relative frecuency(%)
Dust-Surface
f
Relative frecuency(%)
Dust-Free
Surface
g
Relative frecuency(%)
SAE^is (450-700 nm)
Dust-Free Surface
h
Relative frecuency(%)
AAE^col (467-650 nm)

Figure 5

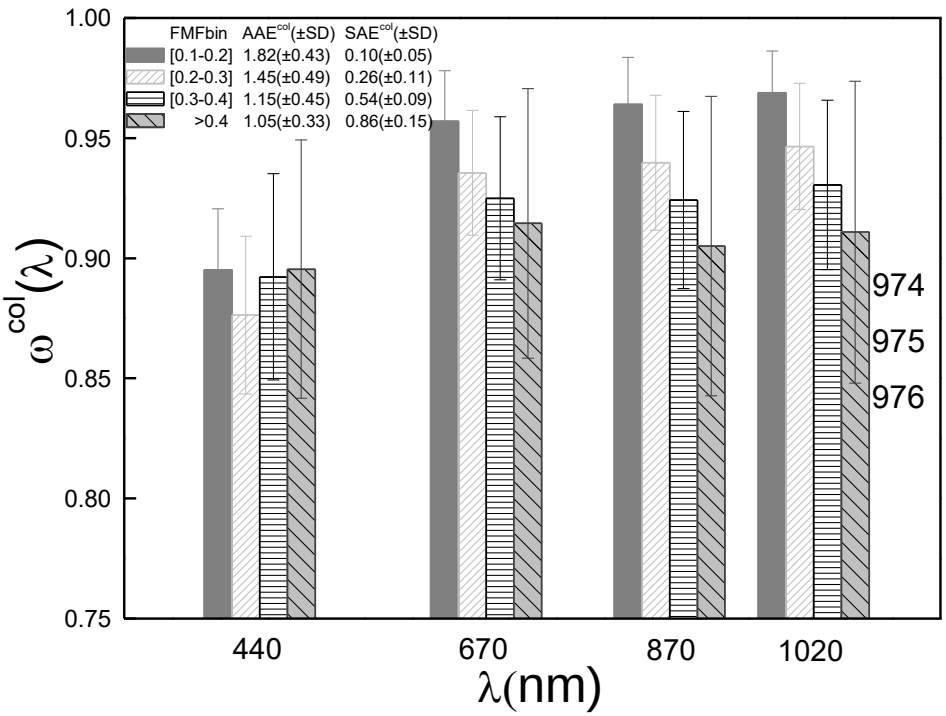
FMFbin AAE^col(±SD) SAE^col(±SD)
[0.1-0.2] 1.82(±0.43) 0.10(±0.05)
[0.2-0.3] 1.45(±0.49) 0.26(±0.11)
[0.3-0.4] 1.15(±0.45) 0.54(±0.09)
>0.4 1.05(±0.33) 0.86(±0.15)
1.00
0.95
0.90
0.85
0.80
0.75
ω^col(λ)
440
670
870
1020
λ(nm)
974
975
976

Figure 6

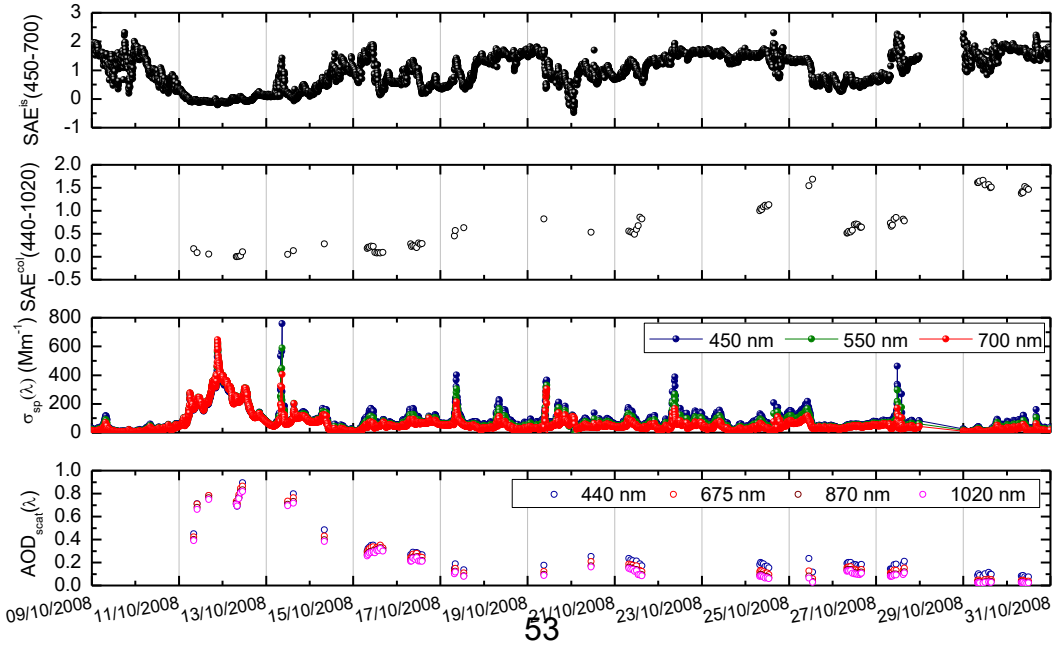
SAE^ls(450-700)
SAE^co(440-1020)
σ_sp(λ) (Mm^-1)
450 nm
550 nm
700 nm
AOD_scat(λ)
440 nm
675 nm
870 nm
1020 nm
09/10/2008
11/10/2008
13/10/2008
15/10/2008
17/10/2008
19/10/2008
21/10/2008
23/10/2008
25/10/2008
27/10/2008
29/10/2008
31/10/2008

Figure 7

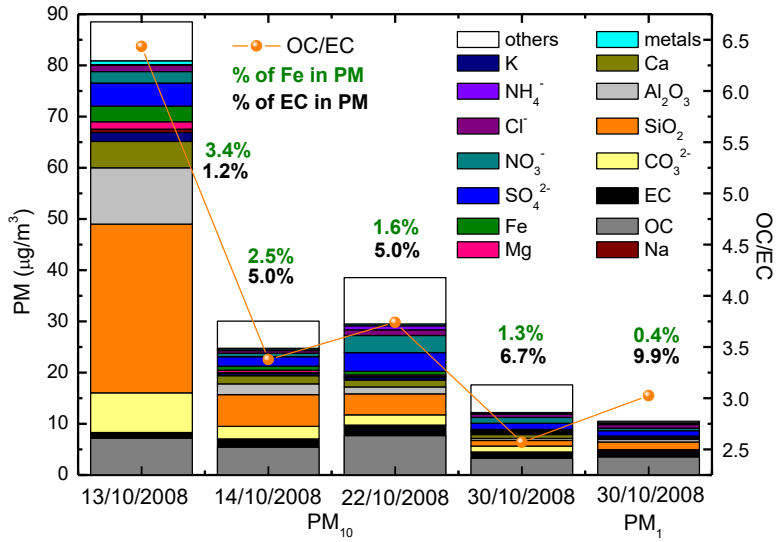
OC/EC
% of Fe in PM
% of EC in PM
others
K
NH4-
Cl-
NO3-
SO4 2-
Fe
Mg
metals
Ca
Al2O3
SiO2
CO3 2-
EC
OC
Na
3.4%
1.2%
2.5%
5.0%
1.6%
5.0%
1.3%
6.7%
0.4%
9.9%
PM (μg/m3)
OC/EC
13/10/2008
14/10/2008
22/10/2008
30/10/2008
30/10/2008
PM10
PM1

Figure 8

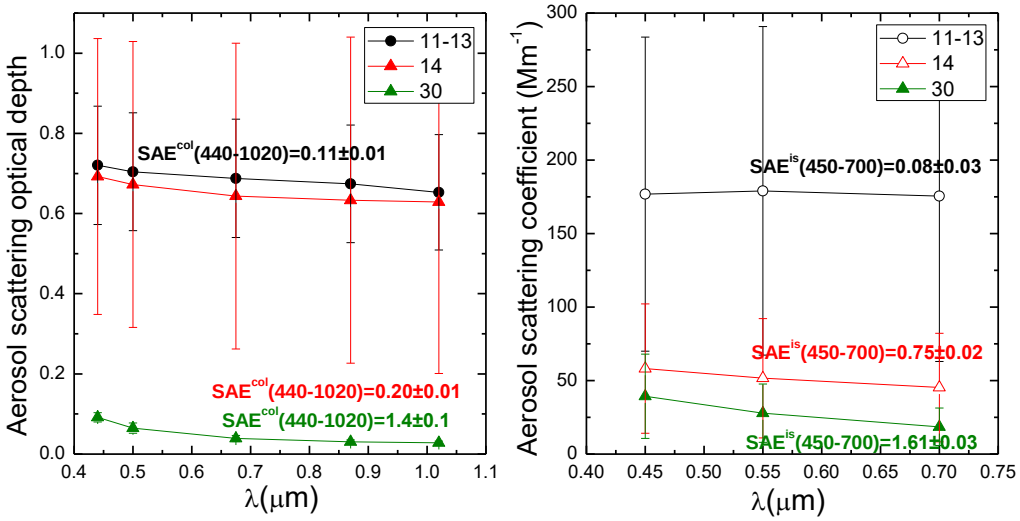

1053

1054

1055

1056

1057

1058

1059

1060

1061

1062

1063

1064

1065

Figure 9

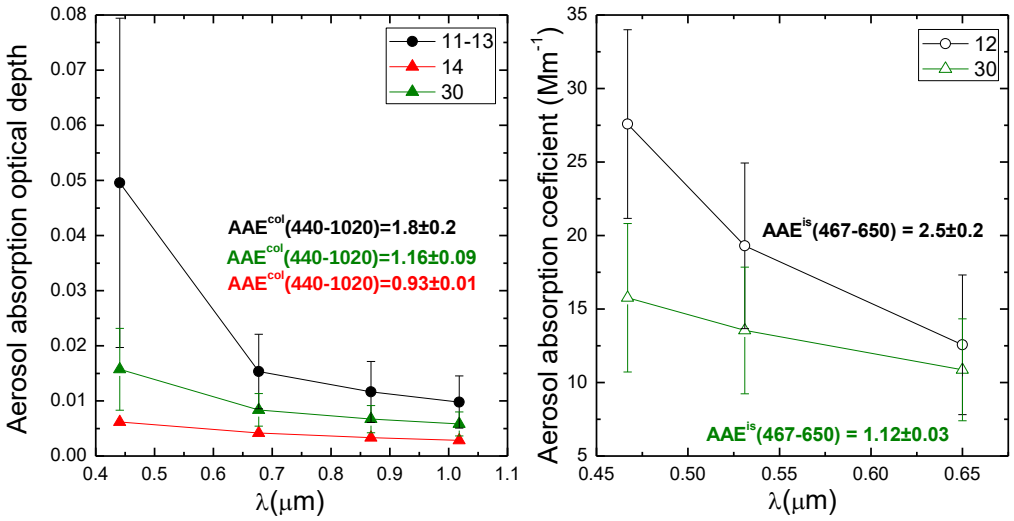
Aerosol absorption optical depth
λ(μm)
11-13
14
30
AAE^col(440-1020)=1.8±0.2
AAE^col(440-1020)=1.16±0.09
AAE^col(440-1020)=0.93±0.01
Aerosol absorption coeficient (Mm^-1)
λ(μm)
12
30
AAE^is(467-650) = 2.5±0.2
AAE^is(467-650) = 1.12±0.03

Figure 10

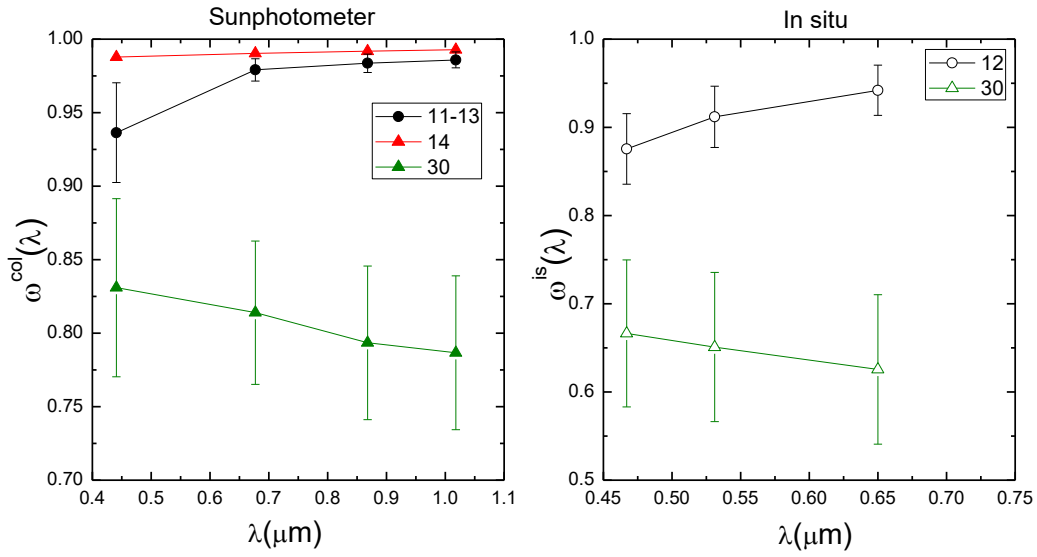
Sunphotometer
In situ
11-13
14
30
12
30
$\omega^{col}(\lambda)$
$\omega^{is}(\lambda)$
λ(μm)
λ(μm)

1092

1093

1094

1095

1096

1097

1098

1099

1100

1101

1102

1103